Possible evidence of nonstatistical properties in the ^{35}Cl$(n, p)^{35}$S cross section

J. C. Batchelder,[1] S.-A. Chong,[1,2] J. Morrell,[1] M. Ayllon Unzueta,[1] P. Adams,[1] J. D. Bauer,[3] T. Bailey,[1] T. A. Becker,[4] L. A. Bernstein,[1,5] M. Fratoni,[1] A. M. Hurst,[1] J. James,[1] A. M. Lewis,[1] E. F. Matthews,[1] M. Negus,[1] D. Rutte,[4] K. Song,[1,6] K. Van Bibber,[1] M. Wallace,[1] and C. S. Waltz[7]

[1]*Department of Nuclear Engineering, University of California, Berkeley, Berkeley California 94702, USA*
[2]*Department of Nuclear Engineering, University of Tennessee, Knoxville, Tennessee 37966, USA*
[3]*Design Physics Division, Lawrence Livermore National Laboratory, Livermore California 94551, USA*
[4]*Berkeley Geochronology Center, 2455 Ridge Road, Berkeley, California 94709, USA*
[5]*Physics Division, Lawrence Berkeley National Laboratory, Berkeley California 94820, USA*
[6]*School of Science, Xi'an Jiaotong University, Xi'an, Shaanxi 710049, China*
[7]*Laser Systems Engineering & Operations Division, Lawrence Livermore National Laboratory, Livermore California 94551, USA*

(Received 30 May 2018; revised manuscript received 27 February 2019; published 25 April 2019)

The ^{35}Cl(n, p) and ^{35}Cl(n, α) cross sections at incident neutron energies between 2.42 and 2.74 MeV were measured using the Berkeley High Flux Neutron Generator. The cross sections for ^{35}Cl(n, p) were more than a factor of 3 to 5 less than all of the values in the neutron absorption data libraries, while the ^{35}Cl(n, α) cross sections are in reasonable agreement with the data libraries. The measured energy-differential cross section is consistent with a single resonance with a width of 293(46) keV. This result suggests that, despite the high incident neutron energy, any attempt to model (n, x) cross sections in the vicinity of the $N = Z = 20$ shell gap requires a resolved resonance approach rather than a Hauser-Feshbach approach.

DOI: 10.1103/PhysRevC.99.044612

I. INTRODUCTION

Nuclear reaction modeling for mid- to high-mass nuclei is treated in different ways depending on the energy range of interest. At low energies the reaction cross section is dominated by specific energy levels (e.g., resonances). This is referred to as the resolved resonance region (RRR). When modelers do not have these data to guide their calculations they rely on other measurements, such as transfer using charged-particle beams, to provide information about the states that could play a role at an equivalent neutron energy. At higher energies, resonances continue to play a dominant role, but they can no longer be individually resolved. In this unresolved resonance region (URR) a new formalism needs to be used. As the energy increases further the number of resonances in a given energy bin becomes large enough that the properties of individual resonances can be treated in a statistical manner using the Hauser-Feshbach (HF) approach [1] where average properties, such as the density of states, can be used.

A good understanding of the energy at which this transition occurs has a direct impact on the design of advanced reactors such as the molten chloride fast-spectrum reactor (MCFR). Recently, TerraPower unveiled the development of a fast spectrum molten salt reactor (MSR) [2]. This design, in order to obtain an adequate fast spectrum, uses chlorides as carrier salt. Chlorine-35 (about 76% of natural chlorine) [3] features a relatively large (n, γ) cross section at thermal energies that is of concern because of the production of the long-lived radioisotope ^{36}Cl. Nevertheless, at the energy range considered for a fast spectrum system (>100 keV), the dominant reaction is ^{35}Cl(n, p). The reaction ^{35}Cl$(n, \alpha)^{32}$P is also open at fast spectrum energies, but has a lower cross section.

In contrast, the ^{37}Cl(n, p) and ^{37}Cl(n, α) reactions have thresholds of 4.08 and 1.57 MeV, respectively, making them better suited for use in a MCFR. For these reasons, designs for chloride-based MSRs foresee the need for high enrichment of ^{37}Cl. A simple neutronics evaluation of the impact of the ^{35}Cl(n, p) cross section in a MCFR revealed that using data from the Evaluated Nuclear Data File (ENDF), ENDF/B-VII.1 as compared to the previous version of the same library, ENDF/B-VII.0, reduces the ^{35}Cl(n, p) effective cross section by almost 45% with a corresponding increase of the multiplication factor of more than 5000 pcm. The change in cross-section data is equivalent to increasing ^{37}Cl to about 50% of the total amount of Cl; therefore, it is of high importance for MCFRs to accurately determine the ^{35}Cl(n, p) cross section in the fast spectrum region.

The isotope ^{35}Cl is noteworthy in that it has a positive Q value for the (n, p) and (n, α) reactions. It is extremely challenging to accurately model (n, p) reactions on light nuclei for a host of reasons, including the large role that resonances play in the reactions and the lack of well-benchmarked proton optical model parameters. This can lead to large uncertainties in the values contained in the ENDF library [4] for these reactions, and a loss in the fidelity of transport calculations for systems where a significant amount of the nuclides is present.

The cross section for the ^{35}Cl$(n, p)^{35}$S reaction has been well measured for neutron energies from 25 meV to 100 keV [5–7]. More recently, Guber *et al.* [8], measured the neutron capture and total cross sections on $^{\text{nat}}$Cl with $E_n = 100$ eV to 600 keV. Above 600 keV, however, there are only three measurements at the D + T (DT) energy of 14 MeV [9–11],

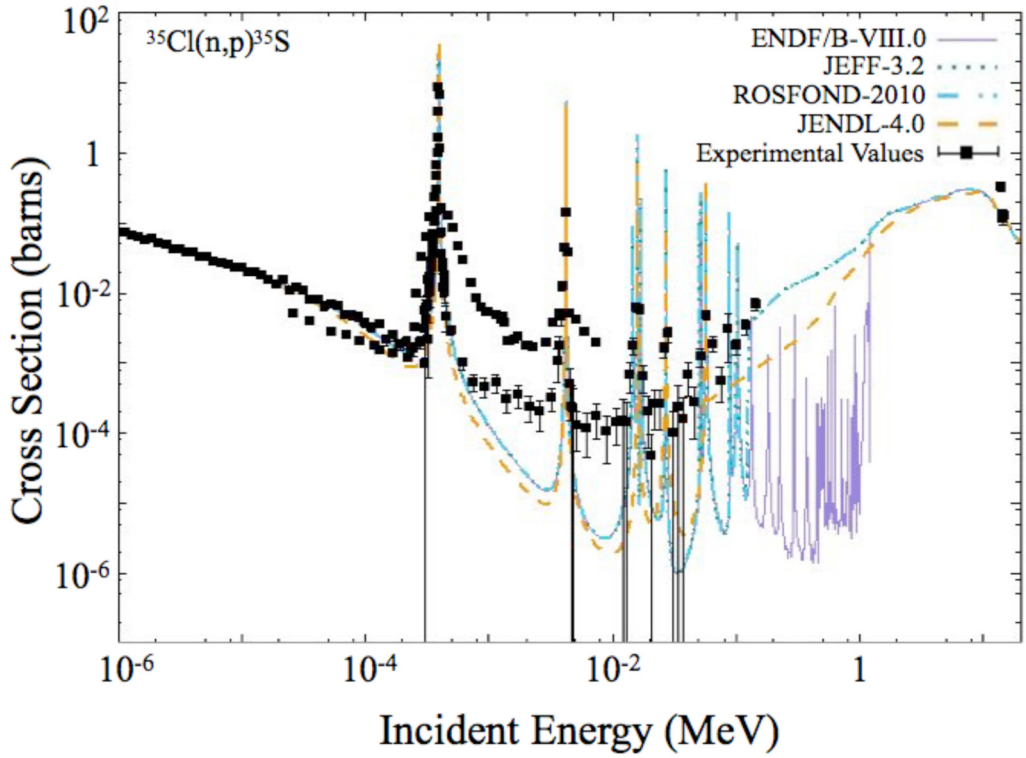

FIG. 1. Comparison of nuclear data libraries for the ^{35}Cl(n, p) reaction and experimental values [5,6,9–11]. Note that ENDF/B-VII.1 is not shown separately as it is identical to ENDF/B-VIII.0.

where "D" and "T" denote "^{2}H" and "^{3}H," respectively. Two of these measurements at 14 MeV agree with each other (131(20) mb [10] and 127(10) mb [11]), whereas a third from Aleksandrov *et al.* [9] has a significantly higher value (330(50) mb) for the cross section.

There are currently no reported measurements of ^{35}Cl(n, p) between 600 keV and 14 MeV where the great majority of the neutrons reside in a fast spectrum system. This has resulted in significant uncertainty between reaction models used to determine the (n, p) reaction cross section in the fast fission energy spectrum. Figure 1 shows a comparison of the ENDF nuclear data libraries for the ^{35}Cl(n, p) reaction along with the measured values. For neutron energies above thermal and less than 50 keV, all the data libraries feature resolved resonances. In the fast neutron region, the databases can be grouped into two sets, with the main difference between them being the treatment of resonances in this region. ENDF/B-VIII.0 [12] and ENDF/B-VII.1 [13] include more realistic detailed resonances between 0.1 and 1.2 MeV, whereas the other libraries, ENDF/B-VII.0 [14], JENDL-4.0 [15], JEFF-3.2 [16], and ROSFOND-2010 [17], feature a smooth behavior as a function of energy for energies above 100 keV. This results in a two to three order of magnitude difference between the two sets of libraries in this energy region. Above 1.2 MeV, all the libraries adopt a smooth trend characteristic of statistical model Hauser-Feshbach [1] calculation.

The detailed resonances between 0.1 and 1.2 MeV were analyzed in Refs. [8,18]. In those works a resonance parameter analysis for cross sections and reaction rates for ^{35}Cl and ^{37}Cl up to 1.2 MeV were performed using the SAMMY parameter covariance matrix code [19]. Using SAMMY, dummy resonances were used to account for resonances in the region where experimental data were not available. In those works, neutron strength functions were calculated for both s and p waves. Chlorine-35 has a ground-state spin of $3/2^{+}$. Consequently, the possible spins for states populated in s-wave capture are 1^{+} and 2^{+}, whereas p-wave capture allows 0^{-}, 1^{-}, 2^{-}, and 3^{-}.

Chlorine-36 is expected to have extremely low level spacing. As a result of this, we expect the entire range of evaluation formalisms, from RRR to URR to HF, to be needed to describe this reaction over the full energy range. In order to minimize the uncertainties in the ^{35}Cl neutron absorption, activation experiments were performed to measure the ^{35}Cl(n, p)^{35}S and the ^{35}Cl(n, α)^{32}P cross sections using the High Flux Neutron Generator (HFNG) on the University of California, Berkeley (UCB), campus.

The nuclear data libraries [12–14,16,17] for the ^{35}Cl(n, α)^{32}P reaction agree with each other with the exception of the JENDL-4.0 evaluation [15], which shows significantly higher values between 2 and 14 MeV that do not match experimental values. The experimental measurements of this reaction consist of ten measurements between 3 and 4.1 MeV [20], a single measurement at 3 MeV [21], and six measurements at 14–14.8 MeV from DT reactions [10,22–25]. Between 4.1 and 14 MeV there are no experimental measurements. The values from Ref. [20] agree well with the data libraries, while the measurements at 14 MeV show a scattering of values between 100 and 191 mb. This is shown in Fig. 2.

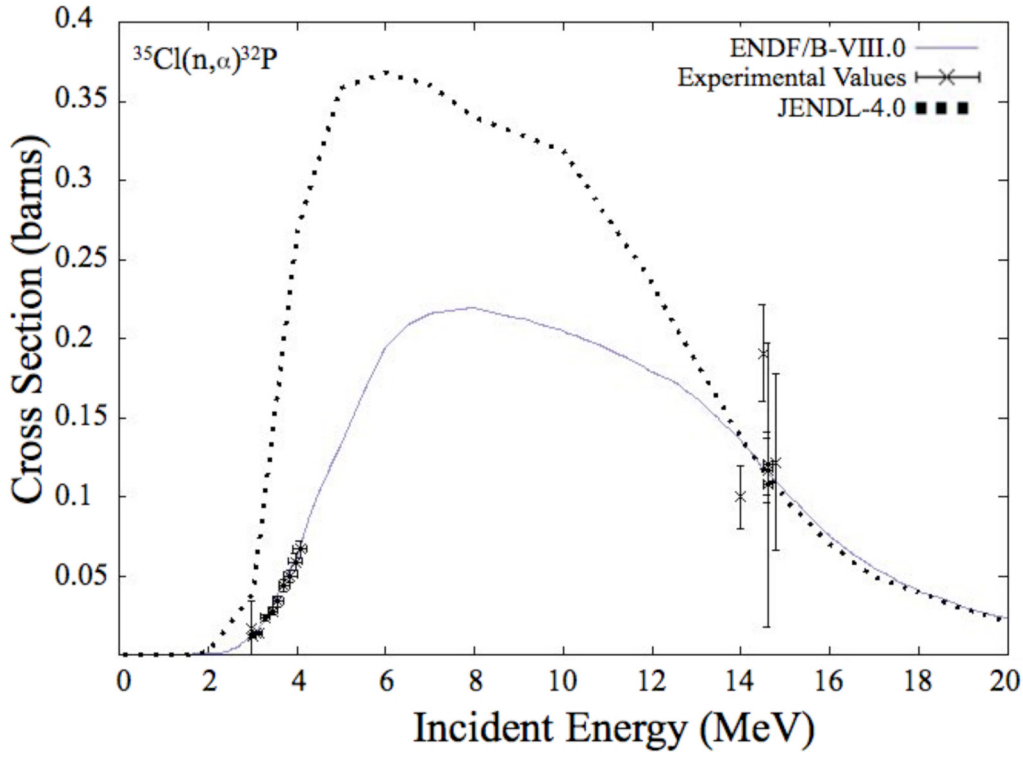

FIG. 2. Comparison of nuclear data libraries for the ^{35}Cl(n, α) reaction. The data libraries ENDF/B-VIII.0, ENDF/B-VII.1, ROSFOND-2010, and JEFF-4.0 [12–14,16,17] all overlap, which matches the experimental values [10,20–25]. The JENDL-4.0 [15] evaluation gives significantly higher values.

II. EXPERIMENTAL DETAILS

The ^{35}Cl$(n, p)^{35}$S and ^{35}Cl$(n, \alpha)^{32}$P cross-section measurements were performed using the Berkeley HFNG located at the campus of the University of California, Berkeley. Pressed pellets of reagent grade NaCl were bombarded with neutrons from the HFNG with an average energy of 2.74(7) MeV at 0° with respect to the beam. The isotopes present in the pellet are ^{23}Na, ^{35}Cl, and ^{37}Cl. Afterwards, the rate of β emission was measured from the sample with a liquid scintillator counter (LSC). At the neutron energies produced by the HFNG, the possible reactions are ^{23}Na$(n, \gamma)^{24}$Na ($t_{1/2} = 15$ h), ^{37}Cl$(n, \gamma)^{38}$Cl ($t_{1/2} = 37$ min), ^{35}Cl$(n, \gamma)^{36}$Cl ($t_{1/2} = 3 \times 10^5$ y), ^{35}Cl$(n, p)^{35}$S ($t_{1/2} = 87.4$ d), and ^{35}Cl$(n, \alpha)^{32}$P ($t_{1/2} = 14.3$ d). Sodium-24 and ^{38}Cl can be eliminated by waiting several half-lives before counting the sample. Chlorine-36 will be present in the sample, but due to its very long half-life, it would not be expected to have a noticeable effect on the rate of β decay of the sample over a counting period of several weeks. This leaves a sample containing ^{35}S and ^{32}P as the only radioactive species observed. Although the major goal of this work is the measurement of the ^{35}S formed via neutron absorption on ^{35}Cl, measuring ^{32}P allows an internal consistency check on the overall measurement.

A. Neutron source

The HFNG (a cutaway illustration is shown in Fig. 3) [26–28] is a self-loading custom D + D (DD) neutron generator. A 100 kV deuterium beam is extracted from an RF-heated deuterium plasma through a nozzle, whose shape was designed to form a flat-profile beam, 5 mm in diameter. The deuterium beam is bombarded on a self-loading water-cooled Ti-coated Cu target. The Ti layer acts as a reaction surface for DD fusion, producing neutrons with a well-known energy distribution as a function of emission angle [29]. The samples to be irradiated are mounted 8.5 mm from the neutron-generating surface at 0°, maximizing the neutron flux at the sample location. During the irradiation, the HFNG

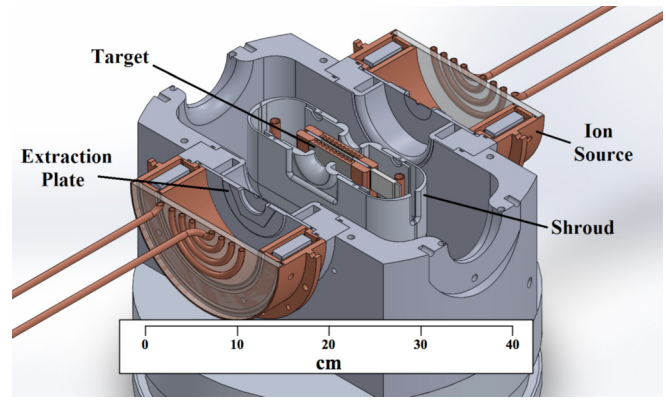

FIG. 3. A schematic of the interior of the HFNG. The slot where samples are located is in the center of the target assembly. Note that the measurements in this paper used only one ion source, resulting in neutrons being produced from only one side.

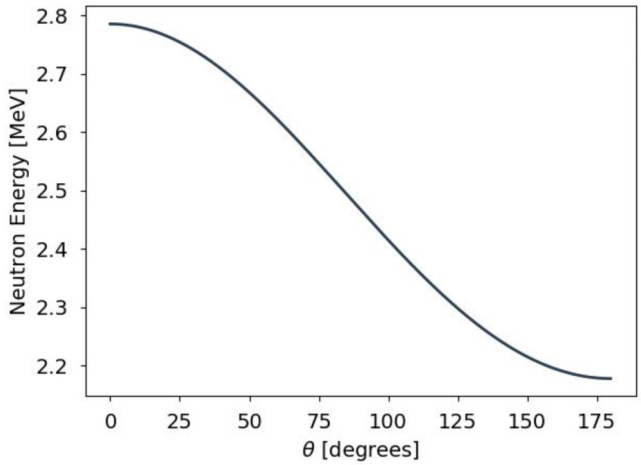

FIG. 4. Energy-angle distribution for neutrons emitted following DD fusion for 100 keV incident deuterons.

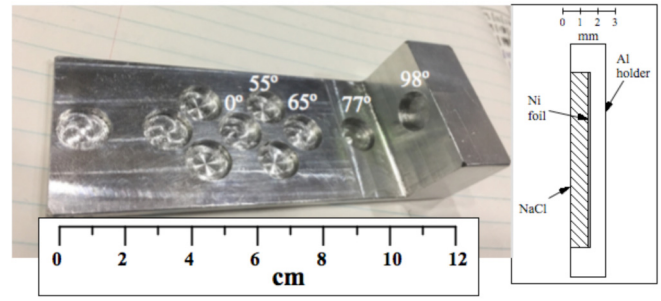

FIG. 5. The multi-angle sample holder used in this work. Samples of NaCl and In (or Ni) foils were placed at 0°, 55°, 65°, 77°, and 98°. The right side of the figure shows a cross-section view with the NaCl pellet and Ni reference foil in place.

voltage and current of the ion source were continuously monitored to keep the neutron flux constant. In addition, a ^{3}He proportional counter was installed next to the HFNG to measure the relative neutron flux at that position. Since this detector is located outside of the HFNG, the neutron flux is very different than what the samples are subjected to, and is only used to verify the stability of the neutron production rate. The absolute neutron fluence is determined through the use of reference foils as detailed below.

To suppress the electrons sputtered off the surface of the Ti, the target is encased in a shroud electrode which is biased at a voltage 2.4 kV more negative than the target (e.g., −102.4 kV if the target is biased to −100 kV). The shroud works by reversing the electric field inside its structure. Without the shroud, the electrons would accelerate back towards the extraction plate, causing overheating and a large flux of bremsstrahlung x rays. Instead, the shroud causes the electrons to experience a force pushing them back towards the target. A more detailed explanation of this technique for secondary electron suppression is described in Ref. [28].

B. Determination of neutron energies

The D(D, n)^{3}He reaction at 100 keV produces neutrons with average energies from 2.18 to 2.74 MeV, over an angular range of 0° to 180° [29]. This is illustrated in Fig. 4. Note that this curve represents monoenergetic neutrons, while in the experiment described in this paper, the curve would have a width due to the deuteron beam slowing down in the target. To take advantage of the variation of neutron energy as a function of angle, an L-shaped sample holder was designed and machined for the multi-angle experiment. With this holder, the samples were held inside the neutron generator, centered at discrete angles with neutron energies spanning between 2.42 (98°) and 2.74 (0°) MeV as shown in Fig. 5.

The approach taken in this work to determine the neutron energy at each position was to use a Monte Carlo N-Particle (MCNP5) [30] model to calculate the neutron flux spectrum for each sample. Using MCNP to calculate the flux spectra accounts for any inelastic scattering or attenuation in the target that might distort the shape of the otherwise ideal DD fusion spectrum.

Table I lists the radius R of each sample disk, as well as the coordinates of the sample inside the HFNG target relative to the origin of the (left side) beam spot. The distances listed in the table were calculated from the design drawings. The sample holder fits snugly inside of the target; as a result, the uncertainties on the distances listed in Table 1 are less than 1 mm. The symbol $\Delta\theta$ is given relative to the incident beam angle.

The source definition used for the MCNP input was generated from the well-characterized energy-angle correlation, where the neutron energy E_n emitted from the D(D, n)^{3}He reaction at a given angle θ can be approximated using the four-term polynomial

$$E_n(\theta) = A_0 + \sum_{n=1}^{3} A_n \cos^n(\theta), \tag{1}$$

where the coefficients used (for 100 kV cathode voltage), $A_0 = 2.4674$, $A_1 = 0.30083$, $A_2 = 0.01368$, and $A_3 = 0.0$, were taken from Ref. [31].

The neutron source definition in the MCNP input was described by a radially Gaussian spatial distribution, which was based both on physical measurements of the heat scaling left by the ion beam spot and on simulations of the ion beam trajectories for the extraction geometry used in this experiment. The calculation takes into account the slowing down of the deuterium primary beam, which reduces the average neutron energy [32]. The beam spot was found to have a 3σ

TABLE I. Positions of each sample in the multi-angle holder. The error on the dimensions is less than 1 mm.

Sample angle	R (mm)	Δx (mm)	Δy (mm)	Δz (mm)	$\Delta\theta$ (deg)
0°	5.5	0.0	0.0	8.5	0
55°	5.5	9.0	8.0	8.5	0
65°	5.5	18.0	0.0	8.5	0
77°	5.5	36.0	0.0	8.5	0
98°	5.5	46.0	0.0	−7.0	90

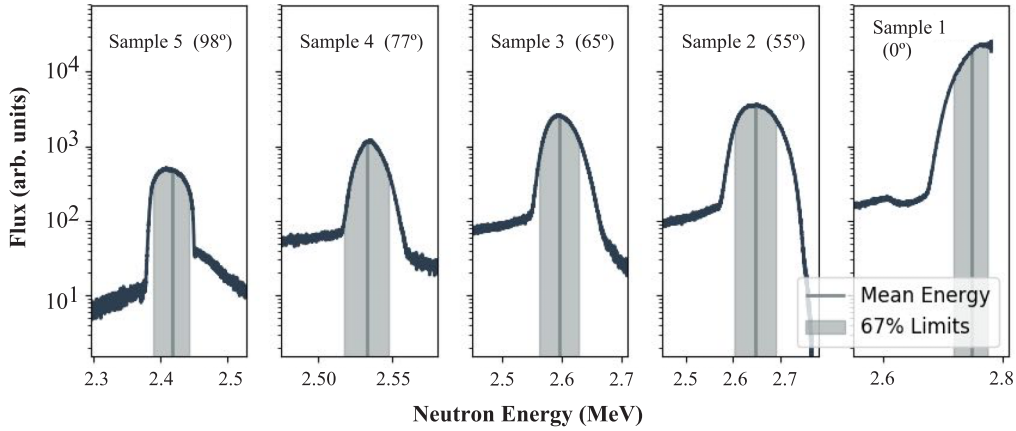

FIG. 6. Energy spectra for the five samples used in this work calculated by MCNP. The standard deviation was found to be symmetric to within 1 keV for each sample, despite the irregular shapes of the distributions.

diameter of about 14 mm, which significantly contributes to the broadening of the flux spectra seen in Fig. 6. Better energy resolution would be difficult to achieve without degraded statistics due to the spectral broadening caused by the beam spot size.

An intensity-angle correlation was also included in the source definition for the MCNP input file, which (similar to the energy-angle correlation) arises from the kinematics of the D(D, n)^{3}He reaction. This correlation is given by Ref. [31] as a fifth-order polynomial approximating the ratio of the neutron intensity I_n at an angle θ to the intensity at 90° as

$$\frac{I_n(\theta)}{I_n(90^\circ)} = 1 + \sum_{n=1}^{5} A_n \cos^n(\theta), \tag{2}$$

where the coefficients (for 100 kV cathode voltage) $A_1 = 0.01741$, $A_2 = 0.88746$, $A_3 = 0.22497$, $A_4 = 0.08183$, and $A_5 = 0.37225$ were also taken from Ref. [31]. The resulting MCNP model was run with 10^9 particles, which gave agreeable statistics in the cells of interest (≈1–2% uncertainties per energy bin).

These simulated spectra were then used to calculate an average energy for each angle. The plots of these calculated energy values are presented in Fig. 6. The values obtained were at 0°, $E_n = 2.74(7)$ MeV; 55°, $E_n = 2.64(7)$ MeV; 65°, $E_n = 2.58(6)$ MeV; 77°, $E_n = 2.52(6)$ MeV; and 98°, $E_n = 2.42(4)$ MeV. Our calculation does not account for energy spread uncertainties in sample distances; however, we can consider those uncertainties negligible with respect to the overall width of the neutron energy spectrum, which is primarily due to the ≈10°–30° angular spread over the beam-spot size and sample diameter (tolerances in distance are on the order of 0.1 mm).

C. Determination of neutron fluence

For a target consisting of N_T target nuclei with a reaction cross section σ_E bombarded with a neutron flux ϕ_E, the rate of production (R) will be

$$R = N_T \sigma_E \phi_E. \tag{3}$$

If this irradiation lasts for some time t_1, and γ-ray counting begins at a later time t_2 and ends at t_3, then the number of decays D with a known decay constant λ during the acquisition will be

$$N_D = \frac{R}{\lambda}(1 - e^{-\lambda t_1})e^{-\lambda t_2}(1 - e^{-\lambda t_3}). \tag{4}$$

The number of γ rays (N_γ) observed is given by

$$N_\gamma = N_D \epsilon_\gamma I_\gamma, \tag{5}$$

where I_γ is the intensity of the emitted γ per decay (i.e., branching ratio) and ϵ_γ is the absolute efficiency of the detection system. Combining Eqs. (3), (5), and (6) gives

$$N_\gamma = \frac{N_T \sigma_E \phi_E}{\lambda}(1 - e^{-\lambda t_1})e^{-\lambda t_2}(1 - e^{-\lambda t_3})\epsilon_\gamma I_\gamma, \tag{6}$$

and consequently

$$\sigma_E = \frac{N_\gamma \lambda}{N_T \phi_E (1 - e^{-\lambda t_1})e^{-\lambda t_2}(1 - e^{-\lambda t_3})\epsilon_\gamma I_\gamma}. \tag{7}$$

This last equation, Eq. (7), can then be used to determine the neutron fluence ϕ_E if the cross section σ_E is known and the cross section if the neutron fluence is known.

The cross sections obtained in this work are relative to the reference reactions, where the neutron fluence is determined via reference reactions. The reference reactions used to determine the neutron fluence in this paper were ^{115}In(n, n')^{115m}In and ^{58}Ni(n, p)^{58}Co.

D. ^{32}P and ^{35}S measurement

A total of three bombardments of NaCl were performed. The first two used a single NaCl pellet at 0° with $E_n = 2.74(7)$ MeV. The third experiment used NaCl pellets at different angles to cover neutron energies from 2.74 to 2.42 MeV. The NaCl pellets were co-loaded with nickel and indium standard foils directly behind the pellets to determine the neutron fluence (see Fig. 5).

Samples of ≈250 mg reagent grade NaCl were pressed into pellets using a hydraulic press, with the resulting pellets having a thickness of 1 mm. In the first two single-energy measurements at 0°, these pellets were co-loaded with metallic

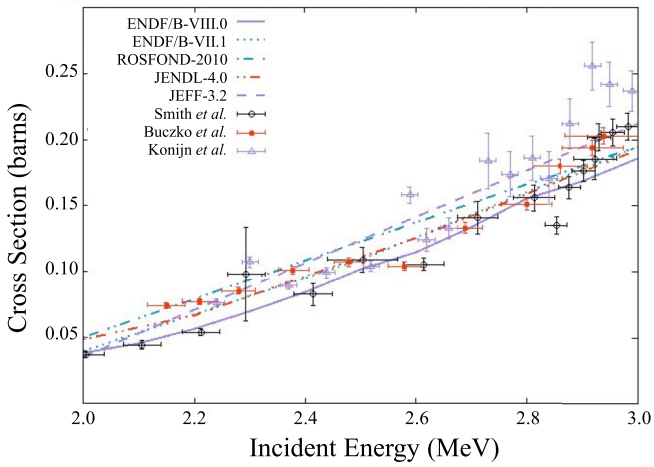

FIG. 7. Experimental (Buczko *et al.* [38], Smith *et al.* [39], and Konijn *et al.* [40]) and evaluated ENDF/B-VIII.0, ENDF/B-VII.1, JEFF-3.2, JENDL-4.0, and ROSFOND-2010 cross section (solid lines) data for ^{58}Ni$(n, p)^{58}$Co for incident neutron energies of 2–3 MeV.

In foils which were used to determine neutron fluence by the IAEA dosimetry standard ^{115}In$(n, n')^{115m}$In reaction [33,34]. In the third multi-energy measurement (multi-angle), a longer irradiation time was needed to get meaningful statistics at the larger angles, so $^{\text{nat}}$Ni foils were co-loaded with the NaCl pellets. In this case, the neutron flux was determined relative to the ^{58}Ni$(n, p)^{58}$Co reaction [13]. The co-loaded foils were located directly behind the NaCl, at a distance of 9.5 mm from the neutron-producing surface.

In the 0° experiments, the NaCl and In were irradiated for 4 h. Energy and efficiency calibration of the high-purity germanium detector was accomplished with a standardized ^{152}Eu source. The cross section of the ^{115}In$(n, n')^{115m}$In reaction is 335(9) mb at the neutron energy of 2.74 MeV. This value is taken from the ENDF/B-VIII.0 evaluation [12], with an uncertainty of 2.6% taken from Capote *et al.* [33]. Based on this, the neutron fluence for the first two 0° experiments were $5.56(16) \times 10^{11}$ and $6.67(17) \times 10^{11}$ n/cm^2 s, respectively.

A major motivation for measuring the ^{35}Cl$(n, p)^{35}$S reaction was to determine if the cross section was a smooth function or showed structure due to resonances. As such, it is important to accurately know the cross section for the ^{58}Ni$(n, p)^{58}$Co at a given neutron energy. There are several experiments in the literature [35–47] that are in the energy range of this work, which show a rather large scattering of values making it difficult to determine if there are resonances in this energy region. However, in this energy range only Refs. [38–40] have a neutron energy spread of less than 200 keV. Of these data sets, the work with the smallest uncertainty in the reported cross section is Ref. [38]. The three data sets are shown in Fig. 7 along with the ENDF/B-VIII.0, ENDF/B-VII.1, JEFF-3.2, JENDL-4.0, and ROSFOND-2010 evaluations. Of these, the ENDF/B-VII.1, JEFF-3.2, and JENDL-4.0 evaluations mostly overlap. The ROSFOND-2010 evaluation is significantly higher than the rest. The newer ENDF evaluation (ENDF/B-VIII.0) is lower by 5–7% than the ENDF/B-VII.1 evaluation. All of the evaluations show a smoothly rising curve in the energy range between 2 and 3 MeV. The data from the three measurements [38–40] show significant deviation from all of the evaluations with a dip in the smooth function between 2.5 and 2.8 MeV. In this paper we report the results of the ^{35}Cl neutron absorption reactions relative to the ^{58}Ni(n, p) reaction with values from both the weighted average of the three measurements [38–40] and ENDF/B-VIII.0.

The results for the measured neutron fluences are given in Table II. The raw number of counts of the γ ray from the reference reaction, N_γ (336.2 keV from ^{115m}In and 810.8 keV from ^{58}Co), the irradiation time T, and the mass of the reference foil, M, are included to show the level of statistics. Note that the sample at 0° was 8.5 mm from the source of the neutrons, while the sample at 98° is 46 mm away. This solid angle is the major cause of the large ratio in the counting rate of 0° to 98°.

The ^{35}S and ^{32}P produced in the irradiation decay solely via the emission of β particles ($Q_\beta = 167$ and 1710 keV, respectively) to the ground state of the daughter. Therefore, a LSC was employed to count the β decays of the isotopes. To prepare the irradiated NaCl for counting, the pellet was first dissolved in 4 ml of water, and then 16 ml of Ultima Gold XR scintillation cocktail was added to the sample and mixed before being counted in the LSC. The LSC used in this study was the TriCarb 2910 TR from PerkinElmer [48].

The LSC was calibrated using standard vials for the efficiency of ^{3}H ($Q_\beta = 19$ keV), 63%, and of ^{14}C ($Q_\beta = 156$ keV), 93%. Sulfur-35 has a $Q_\beta = 167$ keV, which is very close to that of ^{14}C; therefore, we would expect that the efficiency for ^{35}S would be very close to that of ^{14}C. To test this we added 100 nCi of ^{35}S in the form of Na_2S (purchased from PerkinElmer) to a vial with 250 mg NaCl, 4 ml water, and 16 ml Ultima Gold XR. The result of this measurement gave a value of 92.7(7)% efficiency for ^{35}S. Phosphorus-32 has a much larger Q_β of 1711 keV, and the LSC is assumed to have an efficiency of 100% for this isotope.

III. EXPERIMENTAL RESULTS

The irradiated NaCl samples were counted in the LSC three times a week over a 3-month period to separate contributions from ^{35}S ($t_{1/2} = 87.37(4)$ d) [49] and ^{32}P ($t_{1/2} = 14.268(5)$ d) [50] based on the half-life curves. Counting was not started until several days after irradiation to allow any ^{24}Na (formed via the ^{23}Na(n, γ) reaction) present to decay. Each set of samples was counted alongside a "background" solution consisting of the same components but with NaCl that had not been irradiated. The number of counts in the background samples (consistently 0.37–0.42 Bq) were subtracted from the irradiated samples. The resulting half-life curve was then fit as a combination of the two decay curves for ^{35}S and ^{32}P, i.e.,

$$N = N_0(^{32}\text{P})e^{-\lambda' t} + N_0(^{35}\text{S})e^{-\lambda'' t}, \tag{8}$$

where λ' and λ'' are the decay constants for ^{32}P and ^{35}S, respectively. Figure 8 shows the results from the first two

TABLE II. Neutron fluence for the irradiated NaCl samples determined by the reference reactions used in the irradiations. Experiments 1 and 2 used the ^{115}In$(n, n')^{115m}$In reaction, as determined by the yield of the 336-keV γ from the decay of ^{115m}In. This is indicated in column 4 by * next to the number of counts. The fluence was determined using the cross section from ENDF/B-VIII.0 (column 2). Experiment 3 utilized the ^{58}Ni$(n, p)^{58}$Co reaction, as determined by the yield of the 811-keV γ from the decay of ^{58}Co. This is indicated in column 4 by ** next to the number of counts. The fluence for that experiment was determined from both the ENDF/B-VIII.0 cross section for that reaction (column 2) and the weighted average cross section from Refs. [38–40] (column 3).

Expt.	Neutron fluence (cm^{-2})		N_γ (counts)	M (g)	T (h)	θ	E_n (MeV)
	(ENDF/B-VIII.0)	Expt. weighted average					
1	$5.56(16) \times 10^{11}$		3375(58)*	0.2516	4.12	0°	2.74(7)
2	$6.67(17) \times 10^{11}$		3686(61)*	0.2516	4.0	0°	2.74(7)
3	$6.60(8) \times 10^{11}$	$6.42(19) \times 10^{11}$	7566(86)**	0.3275	12.0	0°	2.74(7)
3	$1.49(7) \times 10^{11}$	$1.55(9) \times 10^{11}$	426(21)**	0.0908	11.63	55°	2.64(7)
3	$7.45(55) \times 10^{10}$	$8.0(6) \times 10^{10}$	186(14)**	0.0900	11.63	65°	2.58(6)
3	$2.25(17) \times 10^{10}$	$2.3(2) \times 10^{10}$	183(14)**	0.3273	11.63	77°	2.52(6)
3	$2.80(21) \times 10^{10}$	$2.4(2) \times 10^{10}$	175(13)**	0.3274	11.63	98°	2.42(4)

measurements at 0°. Figure 9 shows the decay curves obtained in the multi-angle measurement.

Once the rate of decay of the given nuclide at time zero (end of irradiation) is determined, the number of nuclei at the end of the irradiation period can be calculated via the standard radioactive decay law: $N = N_0 e^{-\lambda t}$. The cross section σ can then be obtained via Eq. (3). The resulting values for the cross sections of ^{35}Cl(n, p) and ^{35}Cl(n, α) obtained in this measurement are listed in Table III. These values are deduced relative to the reference cross sections taken from the ENDF/B-VIII.0 evaluation [12] for both the single-angle (which used ^{115}In$(n, n')^{115m}$In) and multi-angle (which used ^{58}Ni$(n, p)^{58}$Co) measurements. In addition, the multi-angle measurements are also shown relative to the cross sections of the weighted average of Refs. [38–40] for ^{58}Ni(n, p).

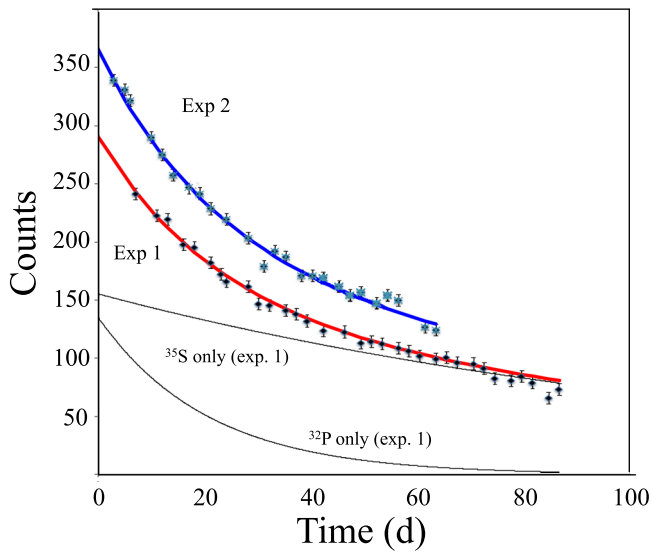

FIG. 8. Raw counts in the LSC resulting from the first two measurements with the LSC. The curve for each experiment is fitted as the sum of the half-life curves for ^{35}S and ^{32}P (see text). This is illustrated for experiment 1.

Estimation of the systematic errors in the cross-section values

The cross sections measured in this work are given relative to the reference reaction used. The discrepancy between the single- and multi-angle measurements is likely due to discrepancies in the value of one of the reference reactions. The ^{115}In(n, n') is a well-known standard reaction with an uncertainty in its cross section of 2.6% [33,34], which is included in the results presented herein. The value for the ^{58}Ni(n, p) reaction is far less certain. However, our assignment of resonantlike behavior is only dependent on the *relative* value of the ^{58}Ni(n, p) cross section over our energy range. Using either the ENDF/B-VIII.0 or the weighted average of the three measurements in this energy range does not alter the cross section's resonantlike behavior.

Table IV lists the ^{35}Cl$(n, p)^{35}$S cross-section values obtained in this work using the neutron fluence based on the ^{58}Ni(n, p) reaction cross section obtained from the ENDF/B-VIII.0, ENDF/B-VII.1, JEFF-3.2, JENDL-4.0, and

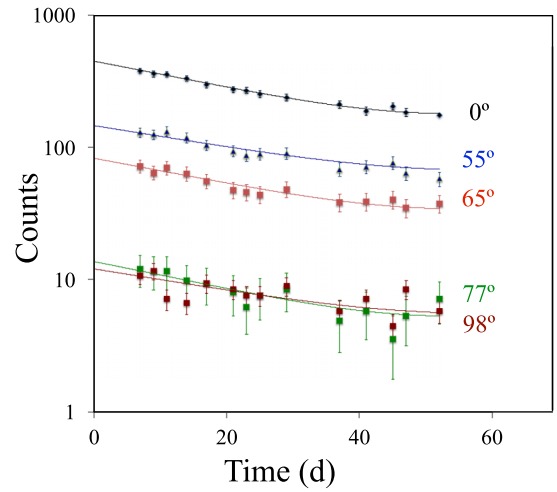

FIG. 9. Half-life curves are shown for the multi-angle ^{35}Cl neutron absorption experiment. The fits are a combination of the two decay curves for ^{35}S and ^{32}P (see text).

TABLE III. Cross-section values for ^{35}Cl$(n, p)^{35}$S and ^{35}Cl$(n, \alpha)^{32}$P obtained in this work relative to ENDF/B-VIII.0 reference reactions and the weighted average of Refs. [38–40] (see text). The corresponding ENDF/B-VIII.0 values (interpolated from Ref. [12]) are shown for comparison.

Expt.	E_n (MeV)	Reference reaction	σ (mb) ^{35}Cl$(n, p)^{35}$S		σ (mb) ^{35}Cl$(n, \alpha)^{32}$P	
			This work	ENDF/B-VIII.0	This work	ENDF/B-VIII.0
1	2.74(7)	^{115}In$(n, n')^{115m}$In	28.4 ± 1.6(stat.) ± 0.3(sys.)[a]	182.6	4.33(28)[a]	7.2
2	2.74(7)	^{115}In$(n, n')^{115m}$In	28.1 ± 1.7(stat.) ± 0.3(sys.)[a]	182.6	4.05(29)[a]	7.2
3	2.74(7)	^{58}Ni(n, p)	31.5 ± 0.5(stat.) ± 0.3(sys.)[a] 32.4 ± 1.2(stat.) ± 0.3(sys.)[b]	182.6	5.2(3)[a], 5.3(3)[b]	7.2
3	2.64(7)	^{58}Ni(n, p)	50.0 ± 3.6(stat.) ± 0.5(sys.)[a] 47.8 ± 3.8(stat.) ± 0.5(sys.)[b]	176.5	5.2(5)[a], 4.5(4)[b]	6.0
3	2.58(6)	^{58}Ni(n, p)	44.6 ± 3.0(stat.) ± 0.5(sys.)[a] 41.7 ± 4.5(stat.) ± 0.5(sys.)[b]	173.1	5.0(7)[a], 4.7(7)[b]	4.7
3	2.52(6)	^{58}Ni(n, p)	26.1 ± 3.5(stat.) ± 0.4(sys.)[a] 25.7 ± 3.6(stat.) ± 0.4(sys.)[b]	169.8	4.7(7)[a], 4.2(7)[b]	3.7
3	2.42(4)	^{58}Ni(n, p)	16.6 ± 5.3(stat.) ± 0.2(sys.)[a] 19.6 ± 5.4(stat.) ± 0.2(sys.)[b]	164.2	1.2(5)[a] 1.4(5)[b]	1.4

[a]Neutron fluence based on ENDF/B-VIII.0 evaluation for the reference reaction.
[b]Neutron fluence based on the weighted average of Refs. [38–40] for the ^{58}Ni(n, p) reference reaction.

ROSFOND-2010 together with a weighted average of the experimental results from Refs. [38–40]. In the range between 2.5 and 3.0 MeV, the ENDF/B-VII.1 and ENDF/B-VIII.0 evaluations disagree by 5–7 % (see Table IV and Fig. 7). The absolute residuals (D) at 2.74 MeV between the cross sections using ^{115}In(n, n') and ^{58}Ni(n, p) as reference reactions (in units of standard deviations) are shown Table IV. The residuals were determined according to $D = |A - B|$, where A is the cross-section value from the experiment using ^{58}Ni(n, p) as a reference reaction, and B is the average (28.3(20) mb) of the experiments using ^{115}In$(n, n')^{115m}$In as the reference reaction.

In this experiment, the NaCl pellets were 1 mm thick with a diameter of 10 mm. The thin reference foil (In or Ni) is located behind the NaCl and is pressed against it (see Fig. 5). The cone of emitted neutrons that hits the NaCl pellet and the reference foil are slightly different. This is referred to as neutron trajectory in Table V. In all of our samples, however, the difference in fluence caused by this is much less than 1%.

In addition, there could be a small difference in the average energy of the incident neutrons from the calculated values due to the deuteron beam being slightly misaligned. This would affect the reference cross section used and therefore the measured cross section for ^{35}Cl(n, p) and the neutron energy. Moving the primary ^{2}H beam by 1 mm in either direction results in our average neutron energy values calculated with MCNP to be shifted by less than 10 keV due to the relatively large ($\approx$14 mm) beam spot. The difference in the value of the cross section changes by $< 1\%$ within 10 keV. The error in the relative Ge detector efficiency has been determined to be 1.2%, and the uncertainty in the foil and pellet weights is

TABLE IV. Experimental cross-section values for ^{35}Cl$(n, p)^{35}$S obtained in this work relative to the cross sections given by ENDF/B-VIII.0, ENDF/B-VII.1, JEFF-3.2, JENDL-4.0, and ROSFOND-2010 ^{58}Ni(n, p) reference reactions and a weighted average of the experimental results from Refs. [38–40] for this reaction. An estimated systematic error of 1% has been added to the error (see text). The absolute residuals (in units of standard deviation, σ_R) between the average (28.3(20) mb) of the first two experiments, which used the ^{115}In$(n, n')^{115m}$In reference reaction at 2.74 MeV, and the corresponding library are given in the last row of the table.

Expt.	E_n (MeV)	σ (mb) ^{35}Cl$(n, p)^{35}$S					
		ENDF/B-VIII.0	ENDF/B-VII.1	JEFF-3.2	JENDL-4.0	ROSFOND-2010	Average [38–40]
3	2.74(7)	31.48(52)	33.5(9)	33.7(10)	37.1(11)	33.27(88)	32.35(13)
3	2.64(7)	50.0(36)	51.9(42)	45.9(37)	58.1(47)	51.8(42)	47.8(39)
3	2.58(6)	44.6(30)	46.0(36)	43.1(34)	51.9(41)	46.1(36)	41.7(46)
3	2.52(6)	26.1(36)	27.1(41)	25.4(38)	30.8(46)	27.5(41)	25.7(37)
3	2.42(4)	16.6(54)	19.2(64)	16.1(54)	21.6(72)	19.6(65)	19.6(54)
		σ_R					
		ENDF/B-VIII.0	ENDF/B-VII.1	JEFF-3.2	JENDL-4.0	ROSFOND-2010	Average [38–40]
		1.5	2.4	2.5	3.9	2.3	1.6

TABLE V. Estimation of systematic errors.

Source	Uncertainty
NaCl/Ni/In weight	$\ll 1\%$
Neutron trajectory	$< 1\%$
Relative detector efficiency	1.2%
D beam position	$< 1\%$

considered to be insignificant. To account for these effects, we added 1% as a systematic error in the neutron fluence values listed in Table II.

The various estimated systematic errors detailed above for this measurement are listed in Table V. The uncertainty introduced by the ^{58}Ni(n, p) cross-section values are by far the largest potential source of systematic error. A small shift in the ^{58}Ni(n, p) cross section at 2.74 MeV could easily explain the discrepancy between the single- (experiments 1 and 2) and the multi-angle measurements (experiment 3) at 0°.

IV. DISCUSSION AND CONCLUSIONS

As mentioned above, the data libraries ENDF/B-VIII.0 [12], ENDF/B-VII.1 [13], ROSFOND-2010 [17], and JEFF-3.2 [16] all agree on the evaluation of the ^{35}Cl$(n, \alpha)^{32}$P reaction, while the JENDL-4.0 [15] library has higher values. There are two groups of experimental cross-section results on this reaction which agree well with the ENDF/B-VIII.0 values. These data are from neutrons with energies from 3 to 4 MeV created via the DD reaction on ^{35}Cl [20,21], and $E_n \approx 14$ MeV arising from neutrons created via the DT reaction [10,22–25]. The values obtained in this work for the energies 2.4–2.6 MeV agree somewhat with the evaluated fit of ENDF/B-VIII.0 (see Table III), with the average value we obtained at 2.74 MeV slightly lower than the evaluated fit. This is consistent with the evaluated fit versus experimental data (from Refs. [20,21]) in the region between 3 and 4 MeV, suggesting that the evaluated fit is slightly too high. This is shown in Fig. 10 with the ENDF/B-VIII.0 evaluation and the previously published data. A close-up of our data in comparison to the ENDF/B-VIII.0 fit is shown in the inset of this figure.

The cross sections measured in this work for ^{35}Cl(n, α) are monotonically rising and agree reasonably well with previous measurements [20,21] and the ENDF/B-VIII.0 evaluation. This supports the statistical model treatment used in the evaluations of this reaction.

The results from our ^{35}Cl(n, p) measurement compared to the ENDF/B-VIII.0 evaluation are shown in Fig. 11, with an expansion of the energy region of interest presented in a linear scale shown in the inset of the figure. Our results from $E_n = 2.42$–2.74 MeV are lower by a factor of 3 to 5 compared to the evaluated value of 164–183 mb from the ENDF/B-VII.1, ENDF/B-VIII.0, JEFF-3.2, JENDL-4.0, and ROSFOND-2010 evaluations. In addition, instead of a smooth curve, our data show structure in the spectrum consistent with a single resonance using the ^{58}Ni(n, p) cross section from both the ENDF/B-VIII.0 evaluation and the weighted average of

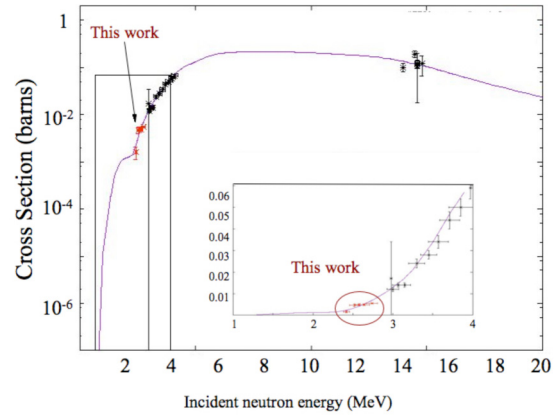

FIG. 10. Comparison of cross-section values of ^{35}Cl$(n, \alpha)^{32}$P from this work (shown in red) to the ENDF/B-VIII.0 evaluation [12] (solid line) and literature values. The values between 3 and 4 MeV are from Refs. [20,21] and the values between 14 and 15 MeV are from Refs. [10,22–25]. The inset shows the energy region of interest in a linear scale. It should be noted that our experimental values from this work that are plotted in this figure are only from the multi-angle measurement (see Table III).

Refs. [38–40]. While this resonance structure is defined by the 0° value, the reference foils and NaCl at this position received the highest dose of neutrons; consequently, the statistics for the γ rays of the reference reaction and the βs from the ^{35}S were the highest of all the data points (see Table II and Fig. 8). Therefore, the cross section values at 0° have the lowest uncertainty of all of the measurements.

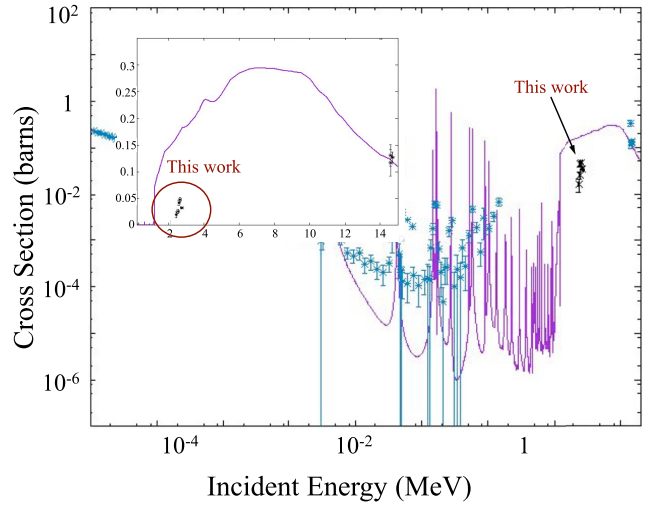

FIG. 11. Comparison of cross-section values of ^{35}Cl$(n, p)^{35}$S from this work to the ENDF/B-VIII.0 evaluation [12] (solid line) and literature values. The values between 10 eV and 100 keV are from Refs. [5–7] and the values between 14 and 15 MeV are from Refs. [9–11]. The inset shows the energy region of interest in a linear scale. It should be noted that the experimental values from this work that are plotted in this figure are from the multi-angle measurement (see Table III).

TABLE VI. Q values and energy thresholds for the $^{35}\mathrm{Cl}+n$ reaction.

Reaction	Q value (keV)	Threshold (keV)
$^{35}\mathrm{Cl}(n,n')$	0.0	0.0
$^{35}\mathrm{Cl}(n,p)^{35}\mathrm{S}$	615.02(5)	0.0
$^{35}\mathrm{Cl}(n,\alpha)^{32}\mathrm{P}$	937.75(5)	0.0
$^{35}\mathrm{Cl}(n,\gamma)^{36}\mathrm{Cl}$	8579.79	0.0
$^{35}\mathrm{Cl}(n,d)^{34}\mathrm{S}$	−4146.24(4)	4265.87(4)
$^{35}\mathrm{Cl}(n,t)^{33}\mathrm{S}$	−9306.17(4)	9574.67(4)
$^{35}\mathrm{Cl}(n,{}^3\mathrm{He})^{33}\mathrm{P}$	−9536.1(11)	9811.2(11)

It is unlikely that the reduction in cross section from 2.64 to 2.74 MeV is the result of a different channel opening up in the $^{35}\mathrm{Cl}+n$ reaction. Table VI shows the Q values and thresholds for this reaction for the lowest energy thresholds. At the energies detailed in this work, the only energetically available reactions are elastic scattering, $^{35}\mathrm{Cl}(n,\gamma)$, $^{35}\mathrm{Cl}(n,\alpha)$, $^{35}\mathrm{Cl}(n,p)$, and $^{35}\mathrm{Cl}(n,n')$. All other reactions have energy thresholds higher than our neutron energies. In addition, there are no known excited levels in $^{35}\mathrm{S}$ that correspond to these energies.

It should be noted that lowering the neutron fluence enough at the highest energy to make the $^{35}\mathrm{Cl}(n,p)$ reaction rise from 2.64 to 2.74 MeV would cause the $^{35}\mathrm{Cl}(n,\alpha)$ cross section value to rise very sharply. The reasonably good agreement of our $^{35}\mathrm{Cl}(n,\alpha)$ with previous experimental data and the evaluated neutron libraries gives us confidence that our results from $^{35}\mathrm{Cl}(n,p)$ are accurate. It should be noted that the $^{35}\mathrm{Cl}(n,p)$ reaction has a positive Q value of 615 keV.

The resonance structure observed between 2.4 and 2.8 MeV in our spectrum implies that a statistical Hauser-Feshbach approach will be inadequate at reproducing the experimental data. Instead, we have fit this region using a Lorentzian model [51] that has the following functional form:

$$\sigma(E_n) = N\frac{\sigma_0 E_n^2 \Gamma_0^2}{\left(E_n^2 - E_0^2\right)^2 + E_n^2\Gamma_0^2}, \tag{9}$$

where E_0, σ_0, and Γ_0 represent the parametrizations determined by the fit for the centroid, width, and intensity of the peak, respectively; N is a peak normalization also determined from the fit. The result of this fit is shown in Fig. 12 with $E_0 = 2.639(9)$ MeV, $\sigma_0 = 200.2(29)$ mb, and $\Gamma_0 = 0.293(46)$ MeV. This result is consistent with a single resonant state centered on 11.22(7) MeV.

Neutron absorption on $^{31}\mathrm{P}$ has been extensively studied, and the $^{31}\mathrm{P}(n,p)$ reaction is well measured from $E_n = 1$–10 and 14–15 MeV. Phosphorus-32 ($Z = 15$, $N = 17$) is similar in structure to $^{36}\mathrm{Cl}$ ($Z = 17$, $N = 19$), with

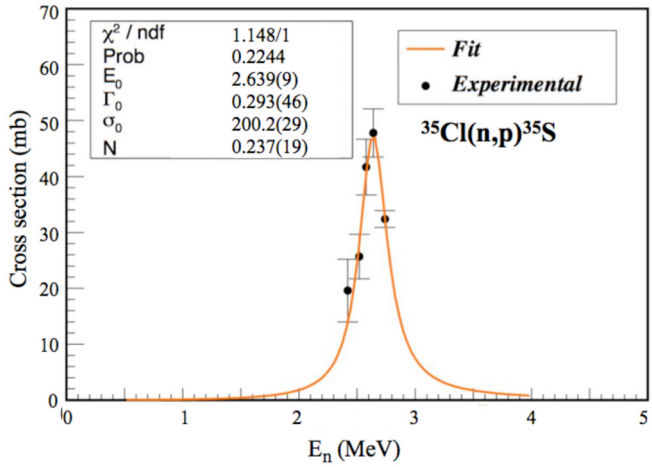

FIG. 12. Lorentzian fit of the resonance in $^{36}\mathrm{Cl}$ observed in the $^{35}\mathrm{Cl}(n,p)^{35}\mathrm{S}$ reaction. The data points for the $^{35}\mathrm{Cl}(n,p)$ reaction are relative to the weighted average of Refs. [38–40] for the $^{58}\mathrm{Ni}(n,p)$ reference reaction (see final column of Table IV).

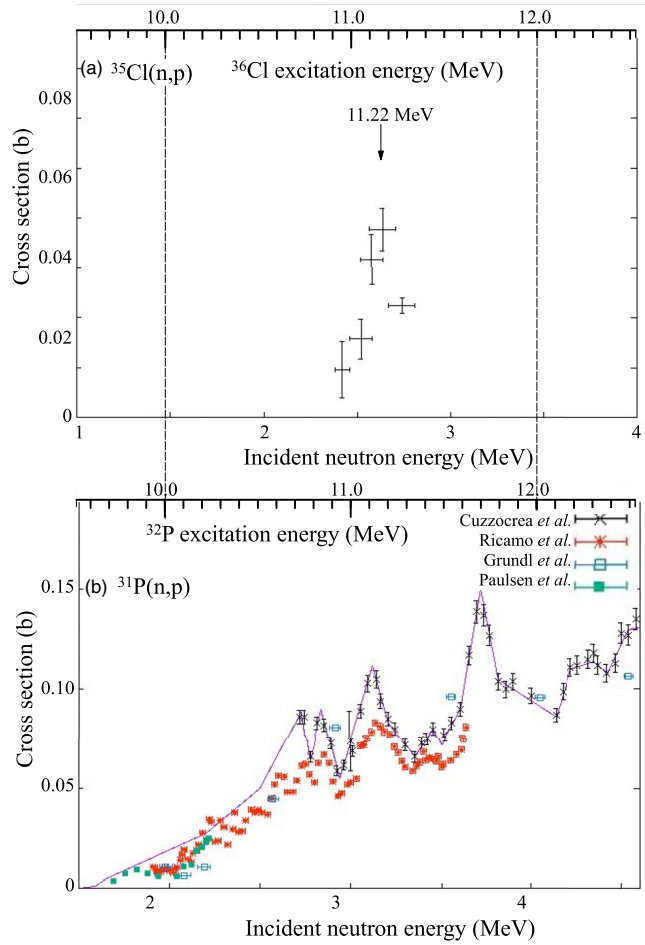

FIG. 13. (a) Close-up of cross sections of $^{35}\mathrm{Cl}(n,p)$ reaction measured in this work. Note that the x axis displays the incident neutron energy on the bottom of the histogram and the corresponding excitation energy of $^{36}\mathrm{Cl}$ on the top. (b) Experimental cross sections of the $^{31}\mathrm{P}(n,p)$ reaction from Cuzzocrea *et al.* [53], Ricamo *et al.* [54], Grundl *et al.* [55], Paulsen *et al.* [56], and the corresponding ENDF/B-VIII.0 evaluation [12], with the same x axes as in (a). The excitation energies of $^{32}\mathrm{P}$ and $^{36}\mathrm{Cl}$ are lined up for comparison. The solid line in (b) is the ENDF/B-VIII.0 evaluation.

$S(n) = 7935.64(4)$ and 8579.79(1) keV, respectively [52]. Figure 13(b) shows the experimental cross-section spectrum arising from the ^{31}P(n, p) reaction fit with the ENDF/B-VIII.0 [12] evaluation. The experimental data [53–56] show peaks in the spectrum with widths and amplitudes similar to our results for ^{35}Cl(n, p). For comparison, Fig. 13 shows our data from ^{35}Cl(n, p) with the excitation energies of ^{36}Cl and ^{32}P lined up for comparison.

In ^{36}Cl the known resonances above the neutron separation energy were obtained through inelastic neutron scattering (n, n'), neutron capture (n, γ), ^{37}Cl$(^3$He$, \alpha)^{36}$Cl [57], and ^{24}Mg$(^{14}$N$, 2p)^{36}$Cl [58] direct reactions. Resonances from the ^{35}Cl(n, γ) and ^{35}Cl(n, n') reactions [18] have been identified using these reactions from the neutron separation energy of 8.58 MeV up to 10.0991 MeV with an average of ≈23 levels/100 keV.

In addition to level density information from the reactions listed above, γ and neutron widths were calculated for ^{35}Cl + n in detail up to neutron energies of 1.485 MeV corresponding to an excitation of 10.065 MeV in ^{36}Cl in Ref. [18]. The neutron widths in this energy region range from slightly less than 1 keV to a few tens of keV (i.e.,, the level at 1353.6 keV has $\Gamma_n = 38.8$ keV). The same work also calculated the wider $\Gamma_n = 621.9$ keV for the much higher incident neutron energy of 7.56 MeV (16.14 MeV excitation energy in ^{36}Cl). The width from our peak in the ^{35}Cl(n, p) cross section is consistent with this trend.

The energy dependence of the cross section we observed is also consistent with the results of Aydin *et al.* [58], who measured the ^{37}Cl$(^3$He$, \alpha)^{36}$Cl reaction populating excited states in ^{36}Cl up to 12.23 MeV. One of the states measured at 11.24 MeV in Ref. [58] is close to the energy of the 11.22(7) MeV peak in our spectrum. If we assume that the energy dependence we observe is due to a single resonance at an excitation energy of 11.22(7) MeV in ^{36}Cl, the width of this resonance is 293(46) keV, with a resulting level lifetime $\tau = \hbar/\Gamma_0 = 2.25(35) \times 10^{-21}$ s. This seems reasonable because at this excitation energy ^{36}Cl is unbound to proton emission by 3.26 MeV and is expected to have a very short lifetime.

In conclusion, we measured the ^{35}Cl(n, p) and ^{35}Cl(n, α) cross sections at incident neutron energies of 2.74(7), 2.64(7), 2.58(6), 2.52(6), and 2.42(4) MeV. The cross sections measured at these energies for the ^{35}Cl(n, p) reaction were a factor of 5 less than the values from the various data libraries. Although additional energy-angle data are desirable, our current measurement indicates the possible observation of a sharply peaked resonance. This result suggests that the cross-section values still display resonance structure at higher energies than what is currently in the evaluated libraries. Therefore, a resolved-resonance treatment rather than an unresolved Hauser-Feshbach approach might be more appropriate in this energy region for evaluation purposes. This may also be true for many other reactions. Future studies using this method of examining cross sections with very narrow energy bins can be used to aid evaluators for a given reaction.

ACKNOWLEDGMENTS

This research is being performed using funding received from the DOE Office of Nuclear Energy's Nuclear Energy University Program. It was carried out at the University of California, Berkeley, and performed under the auspices of the U.S. Department of Energy by Lawrence Livermore National Laboratory under Contract No. DE-AC52-07NA27344 and Lawrence Berkeley National Laboratory under Contract No. DE-AC02-05CH11231. Funding has been provided from the U.S. Nuclear Regulatory Commission, the U.S. Nuclear Data Program, the Berkeley Geochronology Center, NSF ARRA Grant No. EAR-0960138, the University of California Laboratory Fees Research Grant No. 12-LR-238745, and DFG Research Fellowship No. RU 2065/1-1.

[1] W. Hauser and H. Feshbach, Phys. Rev. **87**, 366 (1952).
[2] J. Latkowski, Workshop on Molten Salt Reactor Technologies Commemorating the 50th Anniversary of the Startup of the MSRE, Oak Ridge, TN (unpublished).
[3] M. Berglund and M. Wieser, Pure Appl. Chem. **83**, 397 (2011).
[4] D. A. Brown *et al.*, Nucl. Data Sheets **148**, 1 (2018).
[5] P. E. Koehler, Phys. Rev. C **44**, 1675 (1991).
[6] Yu. P. Popov and F. L. Shapiro, Sov. Phys. Jou. Exp. Theor. Phys. **13**, 1132 (1961).
[7] G. H. E. Sims and D. G. Juhnke, J. Inorg. Nucl. Chem. **31**, 3721 (1969).
[8] K. H. Guber, R. O. Sayer, T. E. Valentine, L. C. Leal, R. R. Spencer, J. A. Harvey, P. E. Koehler, and T. Rauscher, Phys. Rev. C **65**, 058801 (2002).
[9] D. V. Aleksandrov, L. I. Klochkova, and B. S. Kovrigin, Sov. At. Energy **39**, 736 (1976).
[10] W. Nagel and A. H. Aten, Physica (Utrecht) **30**, 775 (1964); **31**, 1091 (1965).
[11] T. Schantl, Thesis, Institut fuer Isotopenforschung und kernphysik, 1970 (unpublished).
[12] https://ndclx4.bnl.gov/gf/project/endf/.
[13] M. B. Chadwick *et al.*, Nucl. Data Sheets **112**, 2887 (2011).
[14] M. B. Chadwick *et al.*, Nucl. Data Sheets **107**, 2931 (2006).
[15] K. Shibata *et al.*, J. Nucl. Sci. Technol. **48**, 1 (2011).
[16] A. J. Koning *et al.*, J. Korean Phys. Soc. **59**, 1057 (2011); https://www.oecd-nea.org/dbforms/data/eva/evatapes/jeff_32/.
[17] ROSFOND-2010: Updated Russian Library of Evaluated Neutron Data, http://www-nds.iaea.org/exfor/endf.html.
[18] R. O. Sayer, K. H. Guber, L. C. Leal, N. M. Larson, and T. Rauscher, Phys. Rev. C **73**, 044603 (2006).
[19] N. M. Larson, J. Nucl. Sci. Technol. **39**, 92 (2002).
[20] H. Alder, P. Huber, and W. Hälg, Helv. Phys. Acta **26**, 349 (1953).
[21] von F. Metzger, P. Huber, and F. Alder, Helv. Phys. Acta **20**, 236 (1947).
[22] V. N. Levkovskii, J. Exp. Theor. Phys. **18**, 213 (1964).
[23] B. E. Bonner, E. B. Paul, and G. C. Phillips, Nucl. Phys. A **128**, 183 (1969).
[24] R. C. Barrall, J. A. Holmes, and M. Silbergeld, Rept: Air Force Spec. Weap. Center Kirtland A.F.B. Repts., AFWL-TR-68-134 (1969).
[25] R. S. Scanlan and R. W. Fink, Nucl. Phys. **9**, 334 (1958).

[26] A. S. Voyles *et al.*, Nucl. Instrum. Methods B **410**, 230 (2017).
[27] C. Waltz, Ph.D. thesis, University of California, Berkeley, 2016 (unpublished).
[28] C. Waltz, M. Ayllon, T. Becker, L. Bernstein, K. Leung, L. Kirsch, P. Renne, and K. Van Bibber, Appl. Radiat. Isot. **125**, 124 (2017).
[29] https://www-nds.iaea.org/public/libraries/drosg2000/.
[30] https://mcnp.lanl.gov.
[31] J. Csikai, *CRC Handbook of Fast Neutron Generators* (CRC Press, Boca Raton, FL, 1987).
[32] M. A. Unzueta, Nucl. Instrum. Methods A **903**, 193 (2018).
[33] R. Capote, K. I. Zolotarev, V. G. Pronyaev, and A. Trkov, J. ASTM Int. **9**, 1 (2012).
[34] E. M. Zsolnay, R. Capote, H. J. Nolthenius, and A. Trkov, IAEA Technical Report No. INDC (NDS)-0616, 2012 (unpublished).
[35] M. Bhike *et al.*, Proceedings of Nuclear Data for Advanced Nuclear Systems, Mangalore, India, 2006 (unpublished), p. TP15.
[36] V. Semkova, V. Avrigeanu, T. Glodariu, A. J. Koning, A. J. M. Plompen, D. L. Smith, and S. Sudar, Nucl. Phys. A **730**, 255 (2004).
[37] T. Shimizu, H. Sakane, M. Shibata, K. Kawade, and T. Nishitani, Ann. Nucl. Energy **31**, 975 (2004).
[38] Cs. M. Buczkó, J. Csikai, S. Sudár, Á. Grallert, S. A. Jonah, B. W. Jimba, T. Chimoye, and M. Wagner, Phys. Rev. C **52**, 1940 (1995).
[39] D. L. Smith and J. W. Meadows, Nucl. Sci. Eng. **58**, 314 (1975).
[40] J. Konijn and A. Lauber, Nucl. Phys. **48**, 191 (1963).
[41] Y. Ikeda, C. Konno, K. Kosako, and K. Oishi, Japanese Report to Nuclear Energy Agency/Nuclear Data Center, Report No. 155, 1990 (unpublished), p. 11.
[42] H. A. Hussain and S. E. Hunt, Appl. Radiat. Isot. **34**, 731 (1983).
[43] M.-W. Wu and J.-C. Chou, Nucl. Sci. Eng. **63**, 268 (1977).
[44] J. K. Temperley, Nucl. Sci. Eng. **32**, 195 (1968).
[45] P. Decowski, W. Grochulski, A. Marcinkowski, K. Siwek, I. Sledzinska, and Z. Wilhelmi, Nucl. Phys. A **112**, 513 (1968).
[46] K. Nakai, H. Gotoh, and H. Amano, J. Phys. Soc. Jpn. **17**, 1215 (1962).
[47] L. Gonzalez, J. Rapaport, and J. J. Van Loef, Phys. Rev. **120**, 1319 (1960).
[48] http://www.perkinelmer.com/CMSResources/Images/46-73886SPC_TriCarb2910TRLSA.pdf.
[49] J. Chen, J. Cameron, and B. Singh, Nucl. Data Sheets **112**, 2715 (2011).
[50] C. Ouellet and B. Singh, Nucl. Data Sheets **112**, 2199 (2011).
[51] M. Herman *et al.*, Reoprt No. INDC(NDS)-0603 BNL-101378-2013 (unpublished), https://www.bnl.gov/isd/documents/82108.pdf.
[52] M. Wang, G. Audi, F. G. Kondev, W. J. Huang, S. Naimi, and X. Xu, Chin. Phys. C **41**, 030003 (2017).
[53] P. Cuzzocrea, G. Pappalardo, R. Ricamo, and F. Vinci, Nuovo Cimento **16**, 450 (1960).
[54] R. Ricamo, E. Luescher, P. Scherrer, and W. Zuenti, Nuovo Cimento **8**, 893 (1951).
[55] J. A. Grundl, R. L. Henkel, and B. L. Perkins, Phys. Rev. **109**, 425 (1958).
[56] A. Paulsen and H. Liskien, Proceedings of the Nuclear Data for Reactors Conference, Paris, 1966, p. 217.
[57] L. Broman, C. M. Fou, and B. Rosner, Nucl. Phys. A **112**, 195 (1968).
[58] S. Aydin *et al.*, Phys. Rev. C **86**, 024320 (2012).